Chemical Methodologies 10(2026) 544-555

Chemical Methodologies

Journal homepage: http://chemmethod.com

Original Article

Kinetic and Mechanistic Investigation of the Reaction between Diethyl Acetylenedicarboxylate and Phthalimide Catalyzed by Triphenylarsine in Alcoholic Media

Halime Kord-Tamandani[1], Younes Ghalandarzehi[2,*]

[1]*Department of Chemistry, Faculty of Science, University of Sistan and Baluchestan, P. O. Box 98135-674, Zahedan, Iran*
[2]*Faculty of Industrial & Mining Khash, University of Sistan and Baluchestan, 98164-161, Zahedan, Iran*

ARTICLEINFO

Article history
Submitted: 2025-12-09
Revised: 2026-01-28
Accepted: 2026-02-06
ID: CHEMM-2512-2065

DOI: 10.48309/chemm.2026.565160.2065

KEYWORDS
Kinetics
Mechanism
UV–Vis spectroscopy
Phthalimide
Diethyl acetylenedicarboxylate

ABSTRACT

In this study, a comprehensive kinetic and mechanistic analysis was carried out for the reaction between diethyl acetylenedicarboxylate (DEAD) and phthalimide in methanolic media using UV–Vis spectroscopy. The effects of temperature, solvent environment, and the structure of dialkyl acetylenedicarboxylates on the reaction behavior were systematically examined. The kinetic data indicated an overall second-order process in which both DEAD derivatives and phthalimide contributed fractional orders close to unity. Further analysis revealed that the second stage of the transformation governs the overall rate of the reaction. Unlike reports employing triphenylphosphine (TPP), where distinct mechanistic pathways were proposed, triphenylarsine (TPA) in this system functions predominantly as an effective nucleophilic catalyst, accelerating the initial interaction and modifying the subsequent mechanistic profile. Thermodynamic parameters (ΔG‡, ΔS‡, ΔH‡, and Ea) were evaluated using temperature-dependent studies, providing deeper insight into the reaction pathway and the associated energy requirements.

* Corresponding author: Younes Ghalandarzehi
E-mail: Younes.ghalandarzehi50@gmail.com

GRAPHICAL ABSTRACT

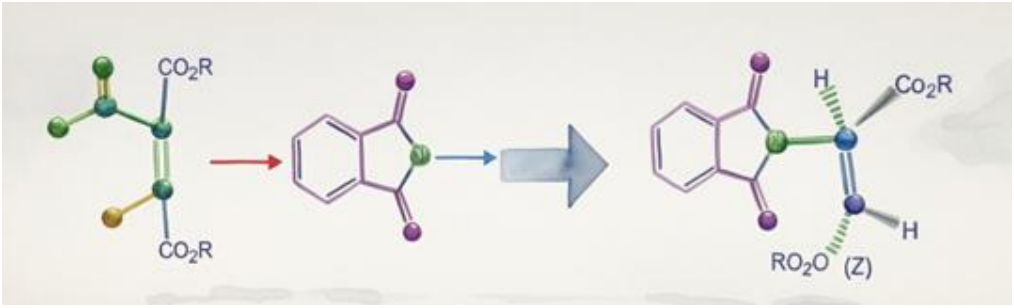

Introduction

N-vinyl heterocyclic compounds constitute essential structural motifs in numerous natural products and exhibit valuable photochemical characteristics [1,2]. These compounds serve as key building blocks in the synthesis of polymeric dyes, polymeric materials, catalysts, natural product analogs, ion-exchange systems, agrochemicals, and pharmaceuticals, and they also find applications in metal separation, extraction of polar compounds, cosmetics, and pigment refinement [3-5]. Members of this compound class have additionally been utilized as promising liquid electrolytes, eco-friendly solvents, and protective functional groups [6-8] .have been explored for their potential as liquid electrolyte candidates, environmentally friendly solvents, and protective functional groups [9]**.** Phthalimide and its N-substituted derivatives constitute a significant category of bioactive species molecules and display a wide spectrum of pharmacological properties, with notable anti-inflammatory, antimicrobial, antitubercular, tumor-inhibitory, antiviral, histone deacetylase (HDAC) activity, and angiogenesis inhibitory properties [10-12].

In fact, the shift from PPh_3 to $AsPh_3$ in the present system highlights the catalytic role of TPA within the reaction medium. Differences in the nucleophilic characteristics of arsenic and phosphorus lead to distinct reaction pathways, ultimately altering the mechanistic sequence. Arsenic exhibits stronger nucleophilicity than phosphorus, which directly influences the course of the reaction.

In ylide structures containing arsenic, the overlap between the arsenic *p*-orbitals and the adjacent carbon orbitals is noticeably weaker than in the corresponding phosphorus ylides. As a consequence, arsenic-based ylides generally show reduced stability and typically appear only as a single observable form, unlike the broader range of phosphonium ylides reported in the literature [19,20]. A preliminary communication of the reaction between DEAD, phthalimide, and TPA was previously reported in a conference abstract. However, that report did not include any kinetic measurements, temperature-dependent studies, activation parameters, solvent effects, or mechanistic analysis. The present study provides the first comprehensive and detailed kinetic and mechanistic investigation of this reaction system (Figure 1).

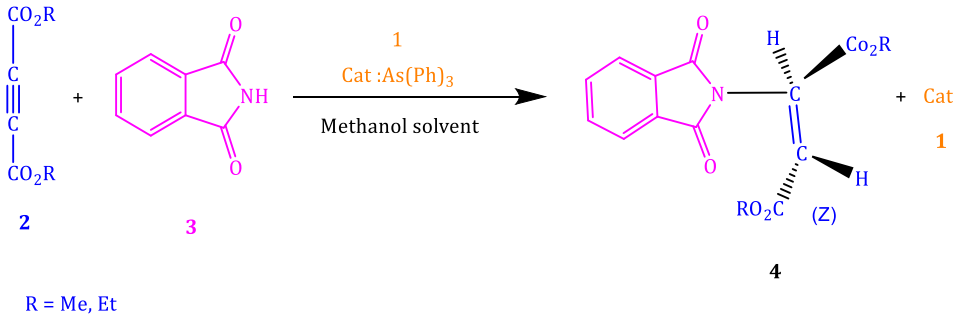

Figure 1: The condensation process involving acetylenic esters and phthalimide carried out in methanol in the presence of TPA as the catalyst

Experimental

General Procedure

Kinetic experiments were performed by following the temporal variation in absorbance with a Cary Bio-300 double-beam UV–Vis spectrophotometer. Before initiating the main measurements, a preliminary scan was carried out to identify a wavelength at which the reaction progress could be monitored reliably. For this purpose, a reaction mixture was prepared in methanol containing 2.5 × 10^{-3} M of compound **1** together with 5 × 10^{-3} M of compounds **2** and **3**. The spectrum of the mixture was then recorded over an appropriate wavelength range to locate a region where product formation produced a measurable signal (Figure 2).

The survey revealed that at 320 nm the starting materials displayed virtually no absorption, which allowed selective detection of the reaction product and minimized spectral interference. Consequently, all subsequent kinetic measurements were performed at 320 nm and under isothermal conditions of 18 °C. Absorbance values were collected as a function of time, providing the data required to construct kinetic profiles for the reaction system (Figure 3).

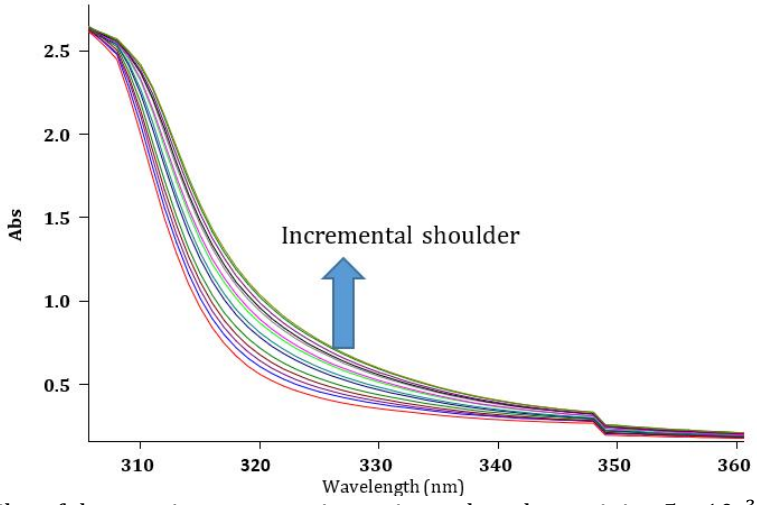

Figure 2: UV–Vis profiles of the reacting system mixture in methanol containing 5 × 10^{-3} M of reactants **2** and **3** and 2.5 × 10^{-3} M of catalyst **1**. The arrow illustrates the gradual increase in product absorption as the reaction proceeds.

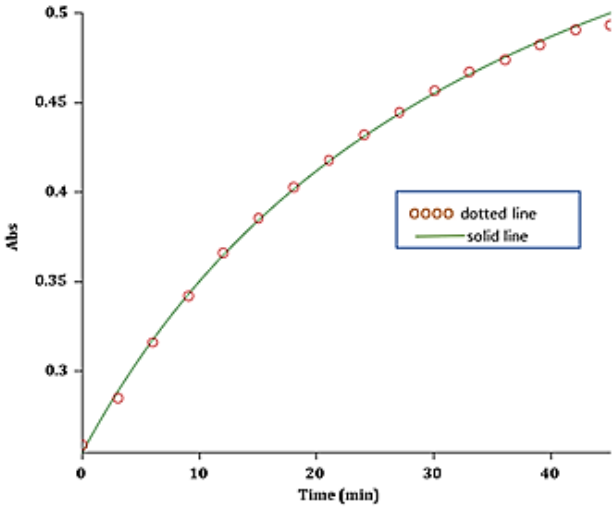

Figure 3: Variation of absorbance at 320 nm with time for the reaction between compound **1** (0.25 × 10^{-2} M) and compounds **2** and **3** (0.5 × 10^{-2} M) in methanol. Experimental measurements are shown as dotted points, while the continuous line represents the kinetic fit.

Figure 3 demonstrates that the measured absorbance over time (depicted by the dotted line) aligns closely with the theoretical curve derived from second-order kinetics (solid line). This strong agreement indicates that the reaction indeed proceeds according to second-order behavior ($\beta + \gamma = 2$). Consequently, the overall reaction rate can be described using the following general kinetic expression (Equation 1):

$$\text{Rate} = k_{ovr}[1]^{\alpha}[2]^{\beta}[3]^{\gamma} \quad (1)$$
$$\text{Rate} = k_{obs}[2][3]$$
$$k_{obs} = k_{ovr}[1]^{\alpha}$$

[1] serves as a constant catalyst, which permits the rate law to be defined.
[2] is a reactant (first order in the rate law).
[3] is the other reactant (first order in the rate law).
The second-order rate constant at 18 °C (k_{ovr} = 6.8 $1/(M^2.min^{-1})$) was subsequently obtained automatically by the software using the standard integrated second-order rate equations [21].

Results and Discussion

Influence of Reactant Concentration

To evaluate the reaction's partial order with respect to the N–H acid (compound **3**), the experiments were conducted under pseudo-first-order conditions using a large excess of DEAD (**2**). The UV–Vis absorbance at 320 nm was monitored over time for a reaction mixture containing **1** (0.25×10^{-2} M), **2** (0.5×10^{-2} M), and **3** (0.25×10^{-2} M) in methanol at 18 °C. Under these experimental settings, the rate of the reaction can be represented by the following kinetic expression (Equation 2):

$$\text{Rate} = k_{ovr}[1]^{\alpha}[2]^{\beta}[3]^{\gamma} \quad (2)$$
$$\text{Rate} = k_{obs}[3]^{\gamma}$$
$$k_{obs} = k_{ovr}[1]^{\beta}[2]^{\gamma}$$

Because the catalyst concentration [**1**] and the excess reagent [2] remain essentially unchanged throughout the reaction, they can be treated as constants in the rate equation. Analysis of the absorbance versus time data at 320 nm (Figure 4) revealed an excellent fit to a pseudo–first-order model, closely matching the experimental observations. This confirms that the reaction is first-order with respect to the N–H, assigning $\gamma = 1$.
Based on prior experiments, the combined reaction orders for reagents **2** and **3** were found to sum to two ($\beta + \gamma = 2$).
Thus, the reaction exhibits first-order behavior with DEAD (**2**), indicating that $\beta = 1$.

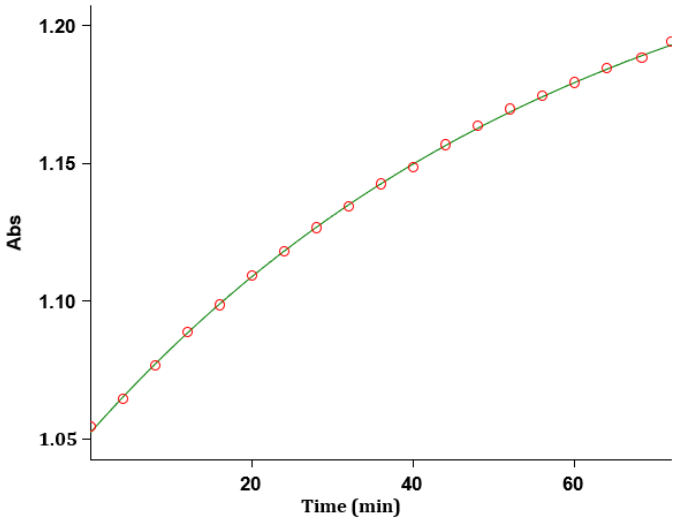

Figure 4: Time-dependent absorbance at 320 nm for the reaction mixture containing **1** (0.25×10^{-2} M), DEAD (0.25×10^{-2} M, acting as catalyst), and the N–H compound (0.25×10^{-2} M) in methanol. Experimental data points are represented by dots, while the solid line corresponds to the fitted kinetic curve.

The Effect of Solvent

To investigate solvent polarity effects, the reaction kinetics were measured in ethanol at 18 °C. A notable decrease in the rate constant was observed (k_{ovr} = 0.75 $M^{-1}.min^{-1}$) relative to methanol (k_{ovr} = 6.8 $M^{-1}.min^{-1}$), consistent with the lower dielectric the value for ethanol (24.5), which is lower than that for methanol (32.7). This behavior can be attributed to the formation of a charge-separated complex in the transition state, which is less stabilized in a lower-polarity solvent due to reduced solvation.

Temperature Dependence and Determination of Activation Parameters

Kinetic studies were carried out at 23, 28, and 33 °C to investigate the influence of temperature on the reaction rate, maintaining identical conditions to prior experiments. The data in Table 1 show an increase in reaction rate with rising temperature, consistent with the Arrhenius equation.

Table 1: Overall reaction rate constants (k_{ovr}, $M^{-1}.min^{-1}$) measured at various temperatures for the reaction of compounds **1, 2**, and **3** under the same experimental conditions

ƛ/nm	Solvent	291 K	296 K	301 K	306 K
320	Methanol	6.8	12.6	23.8	46.1
320	Ethanol	0.75	1.4	2.9	5.8

The reaction kinetics were consistent with the Arrhenius model (E_a[a]), allowing the determination of activation parameters. The activation energy (E_a) and the pre-exponential factor (lnA) were extracted derived from the slope and the intercept, respectively, of the linear ln k versus $1\times T^{-1}$ plot (correlation coefficient r = 0.999), as shown in Figure 5.

While the Arrhenius equation is typically used for gas-phase reactions, the Eyring equation (E_a[c]) offers a more suitable model for capturing how reaction rates vary with temperature in solution. Applying this approach, linearized plots of ln (k/T) versus 1/T and T× ln (k/T) versus T were generated. The activation entropy (ΔS‡) and enthalpy were then extracted from the slopes and intercepts of these graphs (Figures 5-7, and Table 2).

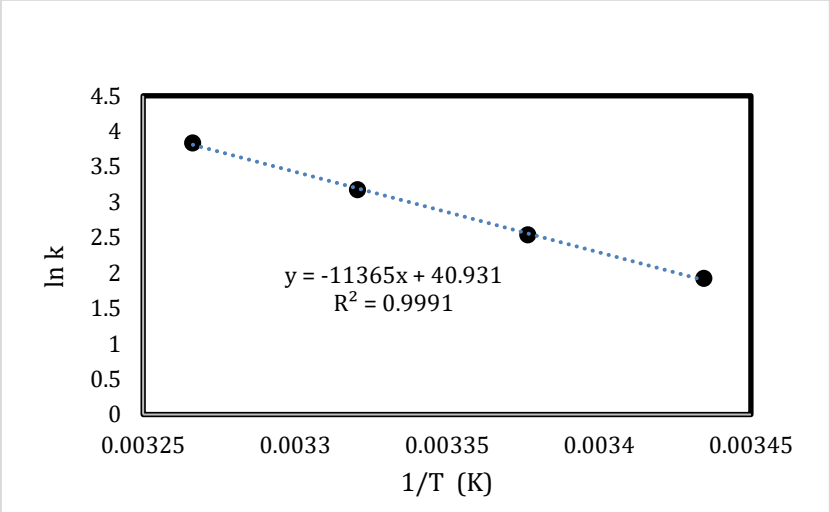

Figure 5: Variation of the second-order rate constant on the inverse of temperature (ln k versus 1/T) for the reaction between compounds **1, 2**, and **3** in methanol, monitored at 320 nm. The observed linear trend is consistent with the Arrhenius equation, allowing calculation of E_a/R from the slope.

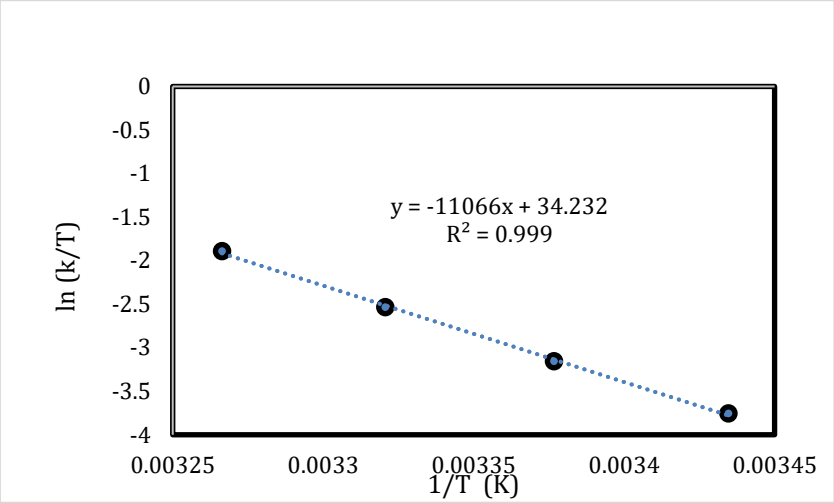

Figure 6: Linearized a plot based on the Eyring relation, (ln(k/T) versus 1/T) pertaining to the reaction, employed to determine the activation enthalpy (ΔH‡) and entropy parameters.

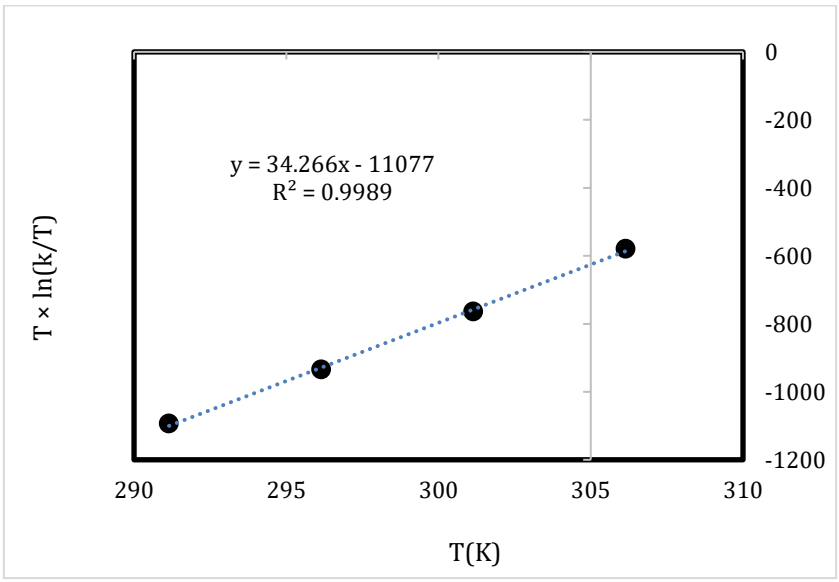

Figure 7: Eyring plot in linearized form (T ×ln k/T versus T) pertaining from the reaction

Statistical evaluation of the Eyring analysis reveals a relationship between the standard deviations of ΔH‡ and ΔS‡, where T_{av} represents the average temperature within the experimental range (Equation 3).

$$\sigma(\Delta S^{\ddagger}) = \frac{1}{T_{av}} \sigma(\Delta H^{\ddagger}) \quad (3)$$

For the majority of solution-phase reactions examined, the standard deviation of ΔS‡ is roughly proportional to that of ΔH‡, following the relation $\sigma(\Delta H^{\ddagger}) \times 0.003\ K^{-1} \approx \sigma(\Delta S^{\ddagger})$. This trend has also been observed in earlier reports [22-24]. The calculated standard errors of the activation parameters are presented together with their respective values in Figures 5 and 6. Beyond estimating the E_a, the E_a^c enables the calculation of the ΔH‡, ΔS‡, and Gibbs free energy (ΔG‡). A clear connection between E_a and ΔH‡ has been established for solution-phase reactions, as described by Equation 4. Fundamentally, the E_a corresponds to the minimum energy a molecule must possess to undergo the reaction.

$$E_a = \Delta H^{\ddagger} + RT \quad (4)$$

The ΔG‡ represents the disparity in energy levels of the transition state and the reactants. Elevated ΔG‡ values indicate that the reaction is under chemical control. As shown in Table 2, the studied reaction exhibits such chemically controlled

behavior. Moreover, high positive ΔG‡ values imply that additional energy is necessary to convert reactants into products. In general, the magnitude of ΔG‡ influences the reaction rate, with larger values corresponding to slower transformations. The Gibbs E_a was calculated using a rearranged form of the Gibbs–Helmholtz equation (Equation 5).

$$\Delta G^{\ddagger} = \Delta H^{\ddagger} - T\Delta S^{\ddagger} \quad (5)$$

The obtained values indicate that the reactions are endothermic, consuming energy. The ΔS‡ provides insight into the molecularity and structural organization of the rate-determining step (RDS), helping to understand the arrangement of species leading to the formation of the transition state.

As shown in Table 2, the ΔH‡ is larger than TΔS‡ in both solvents, indicating that the reaction is enthalpy-controlled rather than entropy-controlled [25]. Nevertheless, the positive ΔS‡ value (≈ +87 $J.mol^{-1}.K^{-1}$) reflects the formation of a relatively loose and dissociative transition state, in which the intermediate has increased degrees of freedom compared to the reactants [26]. Such behavior is consistent with a partially dissociative or charge-separated transition state, where the entropic contribution partially stabilizes the activated complex.

The lnA represents both the frequency of molecular collisions and the proportion of collisions occurring with the correct orientation to form products. Consequently, the values of lnA and ΔS‡ provide further insight into the structural organization and flexibility within the transition state (Equation 6).

$$A = \frac{ekbT}{h} e^{\frac{\Delta S^{\ddagger}}{R}} \quad (6)$$

Entropy values above −10 $J.(mol.K)^{-1}$ generally point to a dissociative reaction pathway. Conversely, strongly negative ΔS‡ values imply that the transition state is more ordered or constrained, which aligns with a mechanistic route involving association.

Furthermore, the activation energies computed from the E_a^a differ from those derived using the E_a^c. Therefore, for accurate determination of activation energies in solution-phase reactions, both the Eyring and Arrhenius formalisms can be applied.

Effect of the Dialkyl Substituent in Acetylenedicarboxylates

This section investigates the effect of the alkyl substituent in dialkyl acetylenedicarboxylates on the reaction rate for the synthesis of *N*-vinyl heterocyclic derivatives. The same kinetic procedure was applied using DEAD and dimethyl acetylenedicarboxylate (DMAD) as reactant **2** under identical conditions (methanol, 18 °C).

The measured rate constants show that replacing DEAD with DMAD "increases the reaction rate", confirming that the alkyl substituent significantly affects the kinetics. These results are consistent with the mechanistic proposal that DEAD participates in the "RDS (step 2)" of the transformation.

Mechanism

Drawing on both the experimental findings and previous literature, a feasible reaction pathway is proposed, as depicted in Figure 8.

Multiple observations indicate that step 2 serves as the RDS of this transformation.

To evaluate this possibility, the rate law was formulated based on the final step of the proposed mechanism depicted in Figure 9 of the desired product (Equation 9):

$$rate = k_5 [I_4] \quad (9)$$

Using the steady-state approximation allows the determination of the concentrations of [I_4, I_3, I_2, and I_1], yielding the following rate law (Equation 10):

$$\text{Rate} = \frac{k_1\ k_2[1][2][3]}{k_{-1} + k_2\ [3]} \quad (10)$$

As Equation 10 excludes k_3, k_4, and k_5, steps 3–5 can be ruled out as the RDS. Given that the rate law

contains k_1 and k_2, the RDS must therefore be selected from between these two steps (Equation 11).

If

$k_1 \rightarrow$RDS ($k_{-1} \ll k_2[3]$) rate = $k_1[1][2]$ (11)

Since compound **1** functions as a catalyst and its concentration does not change, the rate law can be expressed (Equation 12):

$k_{obs} = k_1[1]$ rate = $k_{obs}[2]$ (12)

Equation 12 represents a first-order rate law; however, it does not align with the experimental data, in contrast to the observations described by Equation 1 (Rate = $k_{obs}[2][3]$).

$k_2 \rightarrow$RDS ($k_{-1} \gg k_2[3]$) Rate= $k_2\frac{k_1}{k_{-1}}[1][2][3]$ $k_{obs}= \frac{k_2k_1}{k_{-1}}[1]$ (13)

Since compound **1** acts as a catalyst and its concentration remains effectively unchanged, the rate expression can be written as Equation 1.

Equation 9 is consistent with the experimentally determined rate law (Equation 1), confirming that step 2 (k_2) represents the RDS of the reaction.

The initial step (k_1), which involves the interaction of 1 with 2, occurs very quickly.

Table 2: Thermodynamic parameters of activation for the reaction of compounds **1, 2,** and **3**, measured at 291.15 K

ΔH‡ (kJ.mol^{-1})	**ΔS‡ (J.mol^{-1}K^{-1})**	**TΔS‡ (kJ.mol^{-1})**	**ΔG‡ (kJ.mol^{-1})**	**E_a (kJ.mol^{-1})**
92.00 ± 0.69[c]	87.06± 2.31[c]	25.35 [c]	66.22 ± 1.36 [e]	94.48 [a]
92.10 ± 0.69[d]	87.35± 2.31 [d]	25.43 [d]	66.66 ± 1.36 [e]	94.42 [b]

[a]calculated from Figure 5

[b]obtained from Equation 4

[c]calculated from Figure 6 and from Equation 7: $Ln\frac{k}{T} = -\frac{\Delta H‡}{RT} + \frac{\Delta S‡}{R} + Ln\frac{K_B}{h}$ (7)

[d]calculated from Figure 7 and from Equation 8: $TLn\frac{k}{T} = -\frac{\Delta H‡}{R} + T\left(\frac{\Delta S‡}{R} + Ln\frac{K_B}{h}\right)$ (8)

[e]obtained from Equation 5

This was verified through supplementary experiments carried out specifically on the reaction between TPA (**1**) and DEAD (**2**) under the same reactant concentrations at 18 °C. As shown in Figure 10, the initial reaction between **1** and **2** (step 1) proceeds much faster than the competing steps depicted in Figure 7.

The rate constant for this step, k_1 6.18 (min. M)$^{-1}$, is larger than the observed rate constant for the overall reaction (k_{obs} = 6.8 min^{-1} M^{-1}) involving **1**, **2**, and **3**. Comparison of the total reaction time reveals that the reaction between **1**, **2**, and **3** requires over 100 minutes to reach completion (Figure 3), whereas the reaction between 1 and 2 is completed in less than 2 minutes (Figure 10B).

These observations clearly indicate that the first step is extremely fast relative to the overall process.

Step 3: Step 3 (k_3) involves a rapid intramolecular reaction between the ionic species and C^- in the liquid phase. Step 4 proceeds quickly through a [1,3]-hydrogen shift of I_3, while step 5 (k_5) entails a fast intramolecular transformation within the dipolar intermediate I_4. It is important to emphasize that the overall rate constant, k_{ovr}, in the general rate expression (Equation 10) does not involve k_3, k_4, or k_5, which excludes steps 3, 4, and 5 from serving as the RDS. Taking this into account, step 2 (k_2) is consequently identified as the RDS.

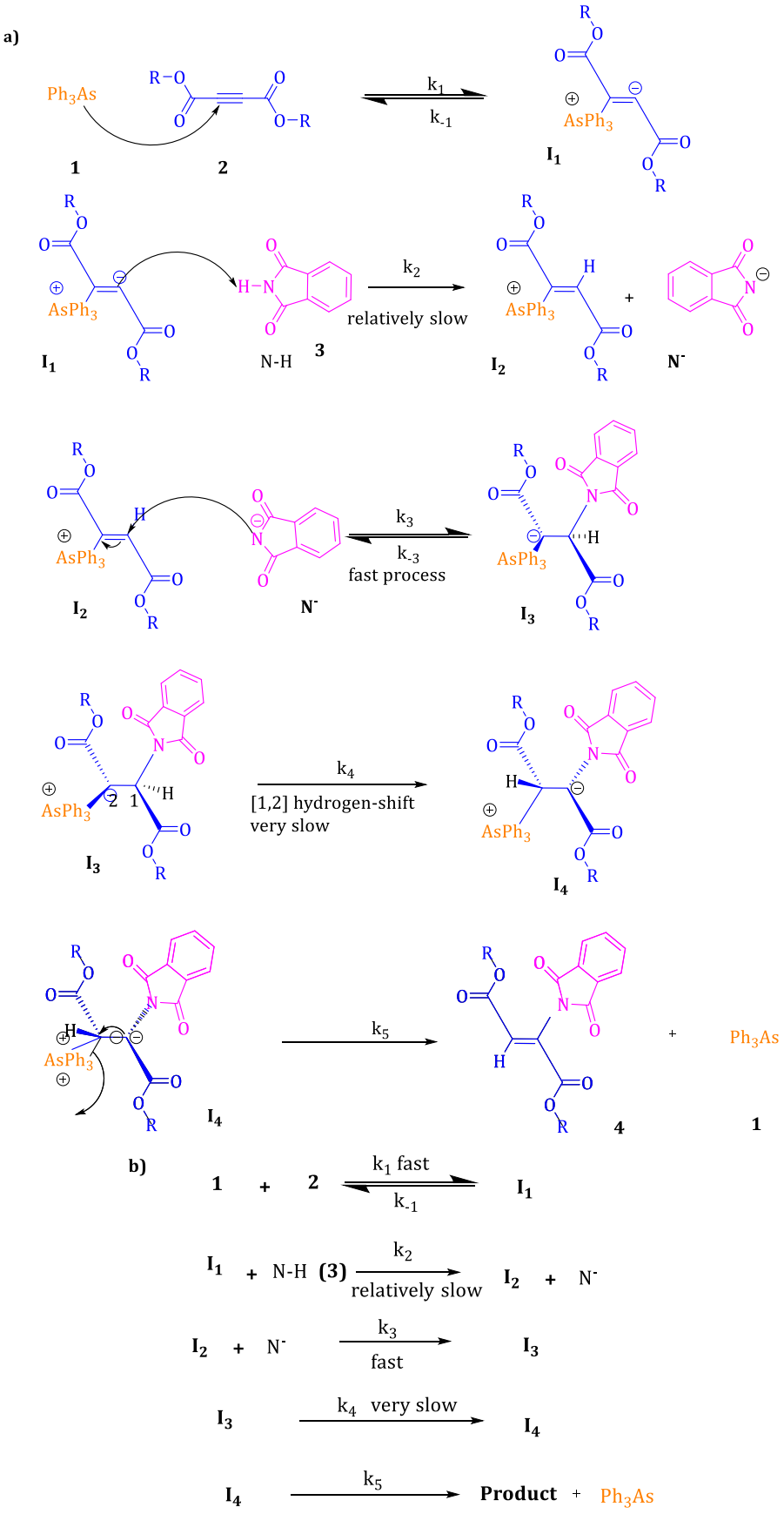

Figure 8: a) Suggested mechanism for the reaction of compounds **2** and **3** catalyzed by compound **1**, leading to the formation of the desired product in methanol b) The simplified scheme for the proposed reaction mechanism

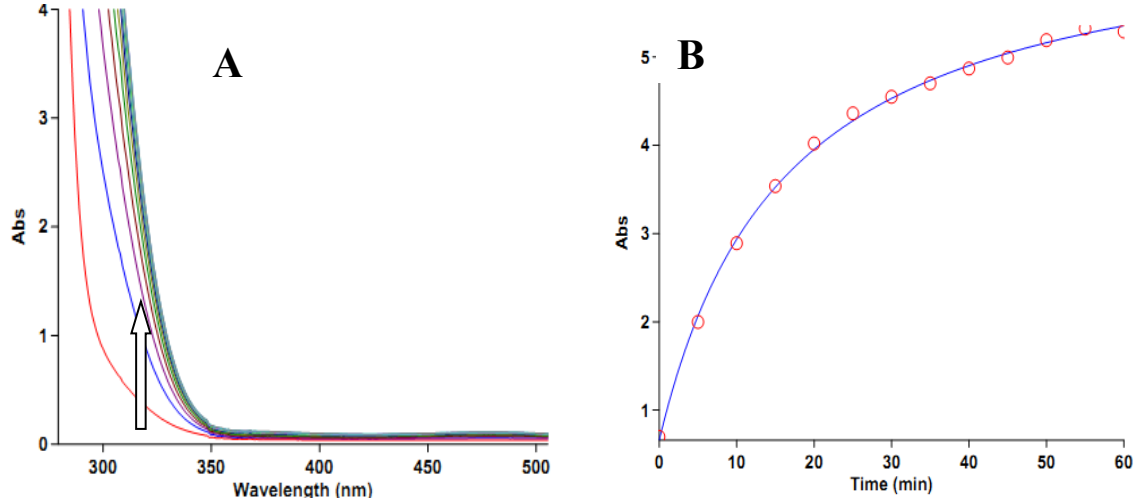

Figure 10: (A) Variation of the absorption spectrum with wavelength at 18 °C for the reaction between compounds **1** and **2** in methanol. The arrow highlights the direction of the reaction. (B) Time-dependent absorbance at 340 nm recorded for the same reaction

Conclusion

Based on the findings, it is concluded that the reaction exhibits overall second-order kinetics, with each reactant contributing a partial order of one. The analysis identifies step 2 as the RDS, with the reaction rate governed by the concentrations of both DEAD and the N–H acid. This contrasts with earlier reports which proposed step 1 as the RDS; the experimental results clarify that while the initial step is influenced by the concentrations of TPA and DEAD, the N–H acid has a negligible effect on its rate. The reaction rate is enhanced by increasing temperature and by employing solvents with higher dielectric constants. A high ΔG‡ indicates that the process is well-controlled from a chemical perspective. Furthermore, investigation into the effect of the dialkyl acetylenedicarboxylate structure revealed that using DEAD instead of DMAD results in a decreased rate constant. This observation confirms the role of step 2 as the RDS, as DEAD participates directly in this decisive step.

Funding

This research was carried out without any financial support from public, commercial, or non-profit organizations.

Conflict of Interest

The authors declares that there were no conflicts of interest related to this work.

Ethical Approval

No ethical approval was required for this study, as it did not involve experiments on human participants or animals.

Authors' Contributions

The sole author was responsible for all stages of the study, including conceptualization, experimental work, data analysis, manuscript preparation, and final approval of the submitted version.

Data Availability Statement

The datasets generated or examined during this research are included in this publication. Further datasets are available from the corresponding author upon request.

Acknowledgments

The author would like to sincerely thank the University of Sistan and Baluchestan for providing

laboratory facilities and instrumental support that enabled the completion of this research.

ORCID

Halime Kord-Tamandani
https://orcid.org/0000-0001-9823-3715
Younes Ghalandarzehi
https://orcid.org/0000-0002-6051-4906

References

[1] Ghorai, D., Tóth, B.L., Lanzi, M., Kleij, A.W. Vinyl and alkynyl substituted heterocycles as privileged scaffolds in transition metal promoted stereoselective synthesis. *Accounts of Chemical Research*, **2024**, 57(5), 726-738.
[2] Nguyen, H.T., Doan, V.T.C., Nguyen, T.H., Tran, M.H. Recent advances in metal-free catalysts for the synthesis of *N*-heterocyclic frameworks focusing on 5- and 6-membered rings: A review. *RSC Advances*, **2025**, 15(13), 9676-9755.
[3] Zhang, X., Bi, W., Cao, Z., Shen, J., Chen, B. Recent developments in the metal-catalyzed synthesis of nitrogenous heterocyclic compounds. *Molecules*, **2024**, 29(22), 5458.
[4] Palomba, M., Dias, I.F.C., Cocchioni, M., Marini, F., Santi, C., Bagnoli, L. Vinylation of *N*-heteroarenes through addition/elimination reactions of vinyl selenones. *Molecules*, **2023**, 28(16), 6026.
[5] Haider, Z., Archana, R., Ju, H. Recent advancements in photocatalytic synthesis of five membered nitrogen heterocycles and their derivatives. *Molecules*, **2025**, 30(17), 3490.
[6] Sivaraj, N., Sakthivel, K., Kikushima, K., Kostić, M.D., Dohi, T., Singh, F.V. Recent advances in non-conventional synthesis of *N*-heterocyclic compounds: emerging strategies and biological perspectives. *RSC Advances*, **2025**, 15(42), 35509-35531.
[7] Zadsirjan, V. Recent advances in the synthesis of six-membered heterocycles via multicomponent reactions (from 2017 to 2022). *Advances in Heterocyclic Chemistry*, **2024**, 142, 283-406.
[8] Hood, J.C., Tshikaya, Y., Manz, A.R., LaPorte, M.C., Klumpp, D.A. Double addition reactions involving vinyl-substituted *N*-heterocycles and active methylene compounds. *The Journal of Organic Chemistry*, **2022**, 87(7), 4908-4911.
[9] Dwivedi, J., Jaiswal, S., Kapoor, D.U., Sharma, S. Catalytic application of ionic liquids for the green synthesis of aromatic five-membered nitrogen heterocycles. *Catalysts*, **2025**, 15(10), 931.
[10] Chi, X., Wang, J., Gao, Q., Zhang, F., Chen, S. The complete chloroplast genomes of two Lancea species with comparative analysis. *Molecules*, **2018**, 23(3), 602.
[11] Ogawa, S., Yazaki, Y. Tannins from Acacia mearnsii De Wild. Bark: Tannin determination and biological activities. *Molecules*, **2018**, 23(4), 837.
[12] Mourad, A.A., Mourad, M.A., Jones, P.G. Novel HDAC/tubulin dual inhibitor: Design, synthesis and docking studies of α-phthalimido-chalcone hybrids as potential anticancer agents with apoptosis-inducing activity. *Drug Design, Development and Therapy*, **2020**, 3111-3130.
[13] Ghalandarzehi, Y., Kord, T.H. Experimental and Theoretical Study on the Mechanism and Kinetics of the Reaction between Hexamethyl Phosphorous Triamide and Dialkyl Acetylenedicarboxylates in the Presence of Benzimidazole. *Chemical Methodologies*, **2023**, 7(10), 776-798.
[14] Talaiefar, S., Habibi-Khorassani, S.M., Shaharaki, M. Comprehensive kinetics and a mechanistic investigation on the biological active pyrano [2, 3-c] pyrazole core in the presence of both eco-friendly catalyst and solvent: Experimental green protocol. *Polycyclic Aromatic Compounds*, **2022**, 42(3), 791-814.
[15] Darijani, M., Shahraki, M., Habibi-Khorassani, S.M. Theoretical study on the mechanism and kinetics of the formation β-carotene epoxides from the oxidative degradation of β-carotene. *Food Chemistry*, **2022**, 389, 133082.
[16] Harada, T., Kubota, Y., Kamitanaka, T., Nakamura, K., Matsuda, T. A novel method for enzymatic asymmetric reduction of ketones in a supercritical carbon dioxide/water biphasic system. *Tetrahedron Letters*, **2009**, 50(34), 4934-4936.
[17] Ziyaadini, M., Maghsoodlou, M.T., Hazeri, N., Habibi-Khorassani, S.M. Novel synthesis of stable 1, 5-diionic organophosphorus compounds from the reaction between triphenylphosphine and acetylenedicarboxylic acid in the presence of N–H heterocyclic compounds. *Monatshefte für Chemie-Chemical Monthly*, **2012**, 143(12), 1681-1685.
[18] Maghsoodlou, M.T., Heydari, R., Habibi-Khorassani, S.M., Hazeri, N., Lashkari, M., Rostamizadeh, M., Sajadikhah, S.S. Triphenylarsine as an efficient catalyst in diastereospecific synthesis of *N*-vinyl heterocyclic compounds. *Synthetic Communications*, **2011**, 41(4), 569-578.
[19] Lloyd, D., Gosney, I., Ormiston, R.A. Arsonium ylides (with some mention also of arsinimines, stibonium and bismuthonium ylides). *Chemical Society Reviews*, **1987**, 16, 45-74.
[20] Yaozeng, H., Yanchang, S. Arsonium Ylides. *Advances in Organometallic Chemistry*, **1982**, 20, 115–157.
[21] Schwartz, L.M., Gelb, R.I. Alternative method of analyzing first-order kinetic data. *Analytical Chemistry*, **1978**, 50(11), 1592-1594.
[22] Chen, L., Poë, A.J. Associative reactions of metal carbonyl clusters: Systematic kinetic studies of some ruthenium and other clusters. *Coordination Chemistry Reviews*, **1995**, 143, 265-295.
[23] Lente, G., Fábián, I., Poë, A.J. A common misconception about the Eyring equation. *New Journal of Chemistry*, **2005**, 29(6), 759-760.
[24] Li, L., Hung, M., Xue, Z. Direct Observation of $(Me_3ECH_2)_5Ta$ (E=C, Si) as the Precursors to $(Me_3ECH_2)_3Ta$: Kinetic and Mechanistic Studies of the

Formation of Alkylidene and Alkylidyne Ligands. *Journal of the American Chemical Society*, **1995**, *117*, 12746–12750.

[25] Wolf, C. Dynamic stereochemistry of chiral compounds: Principles and applications. *Royal Society of Chemistry*, **2007**.

[26] Schwartz, L.M., Gelb, R.I. Alternative method of analyzing first-order kinetic data. *Analytical Chemistry*, **1978**, 50(11), 1592-1594.

Use your device to scan and read the article online

HOW TO CITE THIS ARTICLE

H. Kord-Tamandani, Y. Ghalandarzehi, Kinetic and Mechanistic Investigation of the Reaction between Diethyl Acetylenedicarboxylate and Phthalimide Catalyzed by Triphenylarsine in Alcoholic Media. *Chem. Methodol.*, 2026, 10(5) 544-555

DOI: https://doi.org/10.48309/chemm.2026.565160.2065

URL: https://www.chemmethod.com/article_239999.html